Nanoscale

PAPER

Cite this: *Nanoscale*, 2020, **12**, 4101

Optimization of hydrophobic nanoparticles to better target lipid rafts with molecular dynamics simulations†

Xiaoqian Lin,[a,b] Xubo Lin *[a,b] and Ning Gu *[c]

Received 29th October 2019,
Accepted 10th January 2020

DOI: 10.1039/c9nr09226a

rsc.li/nanoscale

Due to different interactions between lipids and proteins, a plasma membrane can segregate into different membrane domains. Among them, ordered functional membrane domains are defined as "lipid rafts", which play key roles in many biological processes (*e.g.*, signal transduction, endocytosis, *etc.*) in the cell. Hence, it will be of much biological significance to monitor and even regulate the dynamics of lipid rafts. In this work, we designed a ligand-modified spherical nanoparticle with coarse-grained molecular dynamics simulations, which can be encapsulated into the hydrophobic region of the lipid membrane and specifically target either raft or non-raft membrane domains. The preferred localization of the nanoparticle can be tuned by adjusting ligand hydrophobicity, length and density. Generally, more hydrophobic nanoparticles tend to target the raft domain, while less hydrophobic nanoparticles prefer the non-raft domain. Besides, ligand length and density jointly determine the exposure of nanoparticle cores and thus affect the roles of ligands in nanoparticles' final localization. Our results may provide insights into the experimental design of functional nanoparticles, targeting the lipid raft and regulating its dynamics.

Introduction

Over the past several decades, nanoparticles (NPs) have shown great promise in various biomedical applications such as molecular imaging[1,2] and nanomedicines.[3–5] Lots of research studies have pointed out that NPs' physicochemical properties (*e.g.*, size,[6,7] shape,[8–10] hydrophobicity,[11,12] surface modifications,[13–15] *etc.*) can determine their interactions with biological systems, which are essential for NPs' safe and efficient biomedical applications.[16,17] In other words, more efforts will be needed to achieve the controlled synthesis and modifications of NPs with quality control standards,[18,19] which thus enables the tunable nano-bio interactions. Meanwhile, molecular simulations may serve as a powerful tool to facilitate the understanding of the quantitative relationship between NPs' surface physicochemical properties and expected nano-bio interactions.[20,21] For example, by using a series of all-atom (AA) molecular dynamics (MD) simulations, Lu *et al.*[22] found that the adsorption dynamics of serum proteins (*e.g.*, HSA, IgE, and ApoE) onto graphene/gold NPs could be tuned by different surface modifications of hydroxyl groups, which unveiled a simple but robust route to control NPs' protein corona and thus achieve long blood circulation for nanomedicine applications.[23,24] Hence, it is very necessary to use molecular simulations for the optimal design of NPs with designated biological functions.

The plasma membrane, which provides a key platform for the exchange of the matter/signal between the cytosol and the extracellular region, is one of the most important biological systems that have been extensively studied in both molecular simulations[25–27] and experiments.[28,29] Generally, a consensus has been achieved that the plasma membrane can segregate into a series of dynamic and ordered nanoscale membrane domains (termed "lipid rafts") due to differential interactions between lipids and proteins.[30–34] Using model membranes consisting of saturated and unsaturated lipids as well as cholesterol molecules, the exact dynamics of the lipid raft becomes gradually clear.[31–33] The presence of different unsaturated lipids and cholesterol molecules is a prerequisite for the formation of the lipid raft. The *inner-leaflet* dynamics of the raft domain, which affects the partitioning thermodynamics of transmembrane proteins[35,36] and the stability of certain membrane protein oligomers (*e.g.*, H-Ras[37,38]), can be better quantified by the lipid chain order differences.[39,40] The *inter-leaflet*

[a]*Institute of Nanotechnology for Single Cell Analysis (INSCA), Beijing Advanced Innovation Center for Biomedical Engineering, Beihang University, Beijing 100191, China. E-mail: linxbseu@buaa.edu.cn*
[b]*School of Biological Science and Medical Engineering, Beihang University, Beijing 100191, China*
[c]*State Key Laboratory of Bioelectronics, Jiangsu Key Laboratory for Biomaterials and Devices, School of Biological Sciences & Medical Engineering, Southeast University, Nanjing 210096, China. E-mail: guning@seu.edu.cn*

†Electronic supplementary information (ESI) available. See DOI: 10.1039/c9nr09226a

dynamics of the raft domain is mainly determined by *inter-leaflet* coupling.[41] Our previous studies have validated that both the cholesterol flip-flop rate[42] and the lipid chain *cis* double bond position[43] could affect the coupling strength and thus modulate the *inter-leaflet* dynamics of the raft domain. In short, the functions of the plasma membrane are tightly correlated with the raft domain dynamics.

Considering the critical roles of lipid rafts in the functions of the plasma membrane, interactions between NPs and lipid rafts should be an important part of NP–membrane interactions. MD simulation has been widely used to obtain the quantitative molecular interactions,[44–47] which provide a powerful tool for quantifying NP–lipid raft interactions. For example, coarse-grained (CG) MD simulations were successfully used to probe the adsorption and insertion processes of NPs on the phase-separated membrane.[48] Since ultra-small hydrophobic NPs can be easily embedded into the lipid membrane,[49] in this work, we aim to optimize NPs of this kind with CGMD simulations to achieve better targeting of either raft or non-raft domains. Meanwhile, we expect that these ultra-small NPs will not significantly affect the raft domain dynamics. If this is the case, the optimized NPs will be able to be used as bio-imaging agents for the raft domain dynamics, and also have potential to regulate the dynamics of the lipid raft under external stimuli (*e.g.*, thermal effects induced by the NIR laser[50] or the alternating electromagnetic field[51]). Martini CG model,[52,53] which has been widely validated in the lipid raft system,[37,54,55] was used for the optimization process in this work.

Model and methods

Molecular dynamics simulations

The coarse-grained (CG) model, which generally maps several heavy atoms into one interaction site (termed "bead"),[53,56–58] can easily achieve large length scale and long timescale that are very difficult to achieve in all-atom (AA) MD simulations. In this work, the Martini CG model (version 2.0)[53] and GROMACS simulation package[59] were used to study the raft domain systems. The Martini CG model includes four main types of beads: polar (P), apolar (C), nonpolar (N), and charged (Q). Each bead type is further split into 4 or 5 different levels, giving a total of 20 subtypes. More details about this model can be found in the original papers by Marrink *et al.*[52,53] For all the simulation systems, periodic boundary conditions were used in all three dimensions. A cutoff of 1.2 nm was used for electrostatic interactions, which was smoothly shifted to zero from 0 to 1.2 nm. For van der Waals interactions, the Lennard-Jones potential was shifted between 0.9 and 1.2 nm to reduce the cutoff noise with a cutoff of 1.2 nm. The relative dielectric constant was 15, which is the default value of the force field.[52,53] NPs, lipids, and water plus ions were coupled separately to V-rescale heat baths[60] at T = 298 K (coupling constant τ = 1 ps). The systems were simulated at 1 bar pressure using a semi-isotropic Parrinello–Rahman pressure coupling scheme[61] with a coupling constant of τ = 5 ps and compressibility of 3×10^{-4} bar^{-1}. Each simulation was run for 8 μs (effective time, scaling factor of 4 in the Martini model[52,53]) with a time step of 20 fs.

Nanoparticles

In this work, we focused on ligand-modified NPs. As we know, FCC/BCC-packing NPs have been widely used. However, the surfaces of such NPs are not very smooth and isotropic. In order to better quantify the relationship between NPs' surface ligand properties and their membrane partitioning dynamics, the smooth spherical NP core was constructed by evenly distributing Martini CG beads on concentric spherical surfaces with a packing constant of 0.47 nm. The core diameter is ~2.2 nm, which consists of 59 CG beads. To mimic the hydrophobic NP core (*e.g.*, gold NPs[50] and magnetic NPs[51]), C5-type CG beads were employed. Ligands were evenly modified onto the surface of the NP core (Fig. 1). In order to reveal the effects of NPs' surface physicochemical properties on their preferred localization, different ligand lengths and ligand densities as well as two different hydrophobicities (C5 and C1) were studied. Ligand length ranged from 2 to 5 CG beads and the equilibrium distance between two neighboring beads was 0.47 nm. For ligand density, 30%, 60% and 100% modifications were considered. Besides, a more hydrophobic bead (C1) and a less hydrophobic bead (C5) were employed to probe the effect of the NP hydrophobicity.

Lipid bilayers

For the model raft membrane systems, we chose the widely used three-component lipid bilayer consisting of saturated dipalmitoylphosphatidylcholine (DPPC), unsaturated dilinoleoylphosphatidylcholine (DUPC), and cholesterol (CHOL) molecules in a molar ratio of 5 : 3:2.[39,54,63] The Martini-based configurations of these lipids can be found in Fig. 1. The tool *insane.py* developed by Wassenaar *et al.*[64] was used to set up the initial symmetric lipid bilayers with NPs placed inside the center of the bilayers. Each system consists of 1 ligand-modified NP, 590 DPPC, 354 DUPC, 236 CHOL, 21 830 water molecules and 0.15 M NaCl. The initial box size is 20 nm × 20 nm × 10 nm. Then, the simulation systems were run at a high temperature (360 K) after the sufficient energy minimization to achieve a relatively random distribution of lipids and NPs. Finally, each system was gradually cooled down to room temperature (298 K) and experienced a production run of 8 μs. Within the first 2 μs MD simulations, the lipid membrane showed an obvious phase separation as reported,[39,54] which enables us to quantify the partitioning dynamics of NPs between raft and non-raft membrane domains in our simulations. It is worth mentioning that the initial placement of the NP far from the center of the bilayer does not affect NP's preferred membrane localization (Fig. S12†), which validates the feasibility of our simulation system setup.

Analysis of trajectories

Two-dimensional (2D) number-density map. In order to quantify the relative localizations of the raft domain and NPs, the 2D number-density map of DPPC molecules and the

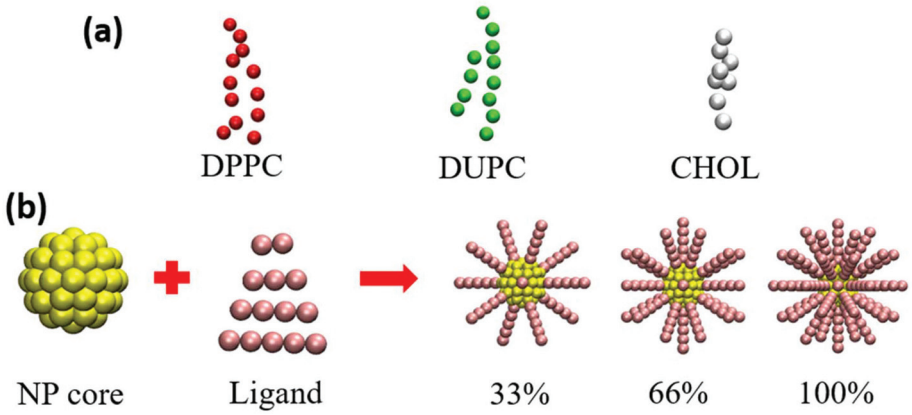

Fig. 1 Schematic illustrations of the CG models of lipids and NPs used in this work. (a) Lipids used in this work: saturated lipids (DPPC), unsaturated lipids (DUPC) and cholesterol (CHOL) molecules. (b) Ligand-modified NPs with different ligand hydrophobicities (C1/C5), lengths and densities. DPPC is colored in red, DUPC in green, CHOL in white, the NP core in yellow, and ligand in pink. All the snapshots in this work are generated by using VMD.[62]

motion tracking of the NP were performed. For the former analysis, the center-of-mass (COM) of DPPC molecules was used. First, all DPPC COM during the last 2 μs trajectory were mapped onto the x–y plane of the lipid membrane. Then, the number density was calculated based on these points on the 2D plane. Finally, all the points were colored according to their number density for visualization. Here, the GROMACS tool *gmx densmap* was employed for this purpose. From this density map, we could clearly differentiate L_o (high probability region) and L_d (low probability region) domains as well as the domain interface (intermediate probability region). The motion of the NP was recorded by black points representing the position of the NP COM during the same period. By overlapping the data from two analyses, we could easily identify NP's relative partitioning preference.

Lipid chain order parameter. Lipid chain order parameter (S_z) was calculated using the following formula:

$$S_{z,n} = \langle \frac{1}{2}(3\cos^2\theta_n - 1) \rangle$$

where θ_n is the angle between the vector connecting the $n-1$ and $n+1$ beads of the lipid tail and the bilayer normal z and S_z is the average of the two chains of the same lipids in the entire bilayer and the designated simulation time.

Cholesterol preference. Considering that DPPC and DUPC molecules have the same number as CG beads, cholesterol preference could be determined directly based on the number of contacts (cutoff: 0.6 nm) of cholesterol molecules with saturated (N_s) and unsaturated lipids (N_{us})[39] as

$$\chi_s = \frac{N_s}{N_s + N_{us}}, \chi_s = \frac{N_{us}}{N_s + N_{us}}$$

where χ_s and χ_{us} are the fraction of cholesterol molecules in contact with saturated and unsaturated lipids.

Voronoi tessellation analysis. In this work, the lipid COM was used for Voronoi tessellation analysis, which partitioned the lipid bilayer plane into polygon regions based on vertical bisector of two adjacent lipids and was achieved by using MATLAB. Each polygon area represents the area of the individual lipid. In visualization, lipid COM was directly colored with this area value for clarity. Hence, the Voronoi analysis was used to quantify the detailed local structural disruption of the lipid membrane by the NP.

Normalized lateral contacts of unsaturated lipids for membrane domain size and stability. For the three-component lipid membrane used in this work, the lateral contacts between unsaturated lipids increase when the lipid membrane changes from the random distribution to the phase separation. In order to compare different systems, the contact number was normalized by the maximum contacts, which was calculated based on the pure lipid bilayer with the same amount of unsaturated lipids. The lateral contacts were calculated separately for each membrane leaflet using GROMACS tool *gmx mindist* with a cutoff of 0.6 nm.

Membrane thickness. In order to obtain the 2D membrane thickness map, 16 × 16 mesh grids were first generated on the x–y plane of the membrane. For the selected period of the MD trajectory, the z coordinate values of PO4-type beads (headgroup) of DPPC and DUPC lipids were averaged separately for the upper and lower membrane leaflets in each mesh grid. The absolute difference between the averaged z coordinate values of the lipid head-groups in the upper and lower leaflets was calculated as the local membrane thickness for each mesh grid. Then, MATLAB was used to generate the 2D membrane thickness map, where the interpolation function was used to reduce the edge effect between the neighboring mesh grids.

Results and discussion

Encapsulation of hydrophobic NPs shows little effects on the lipid raft dynamics

In our simulations, the hydrophobic NPs are embedded in the bilayers with initially a random distribution of lipids and

cholesterol molecules, which can phase separate into stable raft and non-raft domains within the first 2 μs CGMD simulations. As shown in Fig. S1,† the phase separation processes of DPPC/DUPC/CHOL bilayers are not significantly affected by these ultra-small hydrophobic NPs. When the stable phase separation occurs, we could clearly find that the main components of the raft domain are saturated lipids (DPPC) and CHOL, and the non-raft domain is mainly composed of unsaturated lipids (DUPC). The presence of CHOL molecules makes lipid chains of the raft domain much more ordered, while DUPC lipids have more flexible chain conformations in the non-raft domain. We further analyzed lipid chain order parameters (Fig. S2†) and cholesterol preferences (Fig. S3†) in these systems, which are tightly correlated with the dynamics of the lipid raft.[39] Generally, no obvious differences are observed among membrane systems with or without embedded hydrophobic NPs. In other words, these hydrophobic NPs do not significantly affect the lipid raft dynamics, although these may induce local structural disruptions, which will be discussed below. Hence, NPs of this kind will be suitable for targeting raft or non-raft domains with no significant changes to their intrinsic dynamics. In the following few sections, we will discuss how NPs' surface physicochemical properties affect their final preferred localization.

Effects of ligand hydrophobicity and length on the partitioning dynamics of NPs in phase-separated lipid membranes

Here, we considered two different hydrophobicities for the 100% modified ligands. One is Martini "C1" CG bead, which is more hydrophobic; the other is less hydrophobic "C5" bead. Ligand length ranges from 2 to 5 CG beads. The maximum size of ligand-modified NPs is within the limit to be favorable inside the lipid membrane.[13] In order to investigate the roles of ligand hydrophobicity and length in NPs' partitioning dynamics, 2 × 4 different NP–membrane systems were studied separately with 8 μs CGMD simulations. The system snapshots (Fig. 2) and 2D number-density maps (Fig. S5 and S6†) clearly indicated that more hydrophobic NPs tended to reside at the raft domain, while less hydrophobic NPs preferred the non-raft domain. The roles of ligand hydrophobicity here are consistent with those of the transmembrane peptide hydrophobicity in the final membrane partitioning of NPs or peptides.[36,65] The exact molecular mechanism of the role of ligand hydrophobicity in NPs' membrane partitioning thermodynamics can be ascribed to the nonbonded interactions between NPs and lipids/water molecules. Since NPs used here are neutral and hydrophobic, the nonbonded interactions are mainly Lennard-Jones (LJ) interactions. As shown in Table S2,† C1-type beads prefer C1-type beads more, and C5-type beads prefer C5-type beads more. DPPC lipid tails contain only C1-type CG beads, while DUPC lipid tails consist of both C1- and C5-type CG

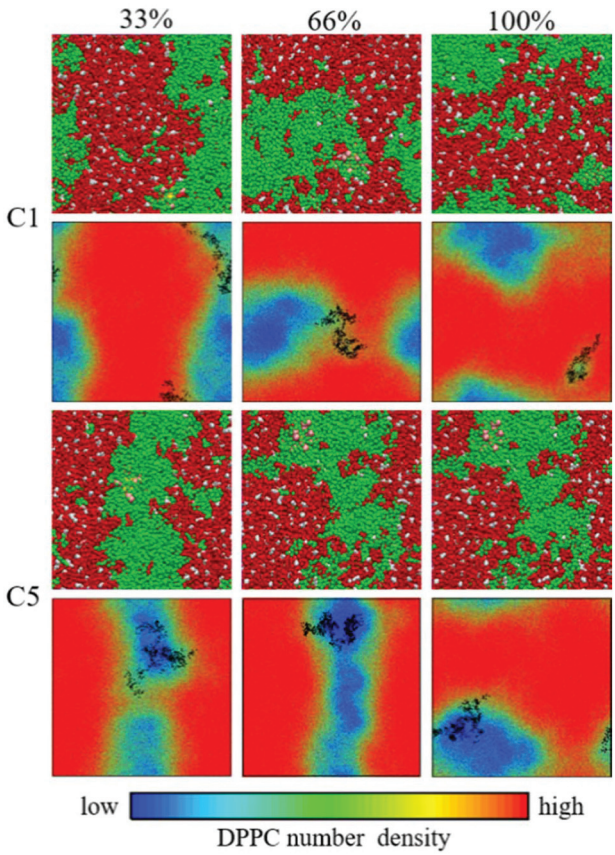

Fig. 3 Effects of ligand density (33%, 66%, and 100%) on the membrane partitioning dynamics of ligand-modified NPs (*n*l = 2). For each ligand hydrophobicity (C1/C5), both the top-view system snapshots (upper panel) of the last frame of 8 μs trajectories and 2D number-density maps (lower panel) are shown. The coloring style is the same as in Fig. 1.

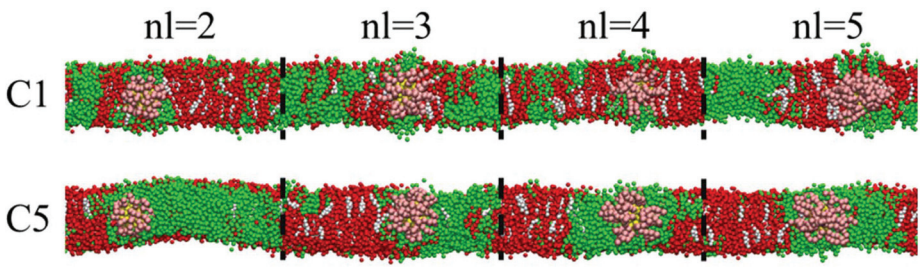

Fig. 2 Effects of ligand hydrophobicity (C1/C5) and length (*n*l = 2, 3, 4, 5) on the membrane partitioning dynamics of ligand-modified NPs (ligand density: 100%). The coloring style is the same as in Fig. 1.

beads. Hence, these differences in interaction determine different membrane portioning thermodynamics of the ligand-modified NPs. Besides, it is worth mentioning that there are always a few DUPC lipids covering the upper and lower parts of NPs when NPs partition into the raft domain. As is known, lipid tails of unsaturated DUPC are much more flexible than those of saturated DPPC. In other words, it is more energy favorable for DUPC lipids to reside at the local curved region where NPs are embedded, which explains the accompanying behavior of DUPC lipids in the NPs' partitioning process.

As for ligand length, we observed no obvious effects of ligand-modified NPs on the final membrane partitioning dynamics (Fig. 2). The reason behind this could be the dense modification density, which completely blocked the exposure of the NP core and made lipids only feel the presence of ligands. In other words, if we reduce ligand density, we probably could see different partitioning dynamics for the embedded NPs. Hence, we further investigated the roles of ligand density in NPs' membrane partitioning dynamics.

Roles of ligand density in the membrane partitioning dynamics of NPs in phase-separated lipid membranes

In addition to ligand density (100%), we also consider the other two ligand densities (33% and 66%). The last 2 μs of each 8 μs trajectory was selected for analysis, because NPs' partitioning dynamics in the phase-separated lipid membrane during this period reached the proper equilibrium for statistics. As shown in Fig. S3 and S6,† for less hydrophobic NPs ("C5"), no matter how you changed the ligand density and length, NPs were always located in the non-raft domain. However, for more hydrophobic NPs ("C1"), ligand density did affect NPs' membrane partitioning dynamics, especially when the ligand was relatively short (nl = 2). Based on the system snapshots and 2D number-density maps (Fig. S3 and S5†), we could find that the raft preferences of more hydrophobic ligand-modified NPs were gradually shifted to the non-raft domain by reducing ligand density in the case of short ligands.

For ligand-modified NPs, flexible ligands can collapse onto the surface of the NP core to prevent the surface exposure.[66–69] The degree of the exposure is regulated by ligand length and density. Longer ligand length and higher ligand density may lead to absolutely no exposure, which makes the NP core "hidden" inside. In our studied systems, for less hydrophobic ligands ("C5"), since the hydrophobicity of ligands and the NP core ("C5") are the same, the exposure of the NP core will not change NPs' interactions with their surrounding lipids. Thus, NPs' non-raft preferences will not be changed in this case. In the case of more hydrophobic ligands ("C1"), C1 CG beads have preferred interactions with the raft domain lipid tails.[36] Hence, a certain exposure of the NP core will weaken the interactions between ligand-modified NPs with the raft domain

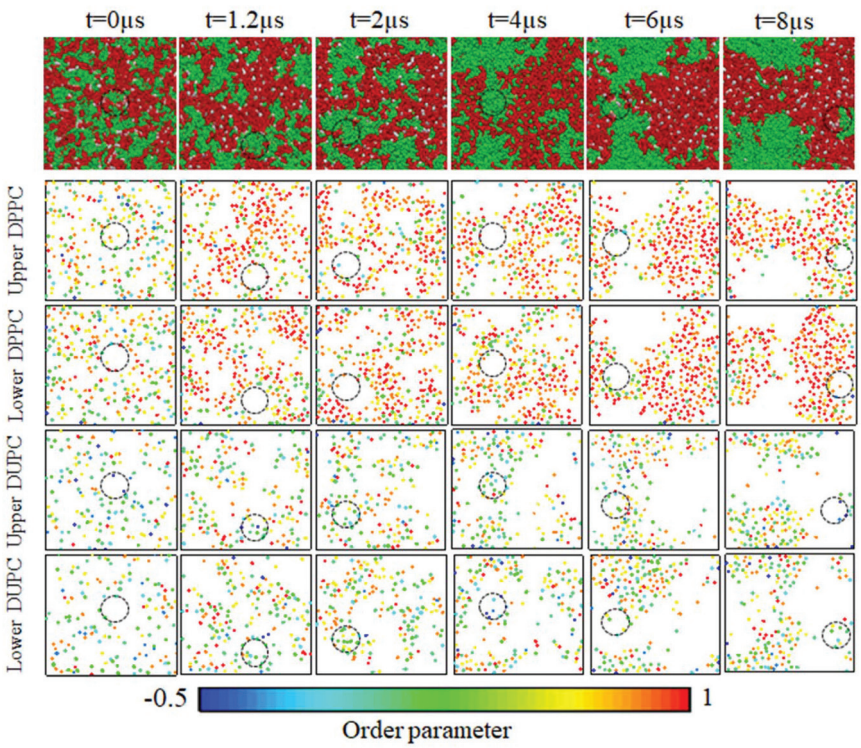

Fig. 4 System snapshots and time evolutions of lipid order parameters for each lipid of NP-embedded lipid membrane systems (ligand hydrophobicity: C1, ligand length: nl = 5, and ligand density: 100%). Each point represents one DPPC/DUPC molecule, and its color shows the averaged chain order parameters. The dashed black circle indicates the localization of the ligand-modified NP. The coloring style of system snapshots is the same as in Fig. 1.

lipids, which inevitably reduces NPs' raft affinity. In the case of low ligand density, the collapse of short ligands onto the surface of the NP core cannot compensate the presence of free space on the surface of the NP core, which provides more chances for direct lipid–NP core interactions. Then, the attractive interactions of ligand-modified NPs with non-raft domain lipids became comparable with those with raft domain lipids. Hence, differences in the preferences of the ligand-modified NPs to either the raft or non-raft domains became no longer obvious (Fig. 3).

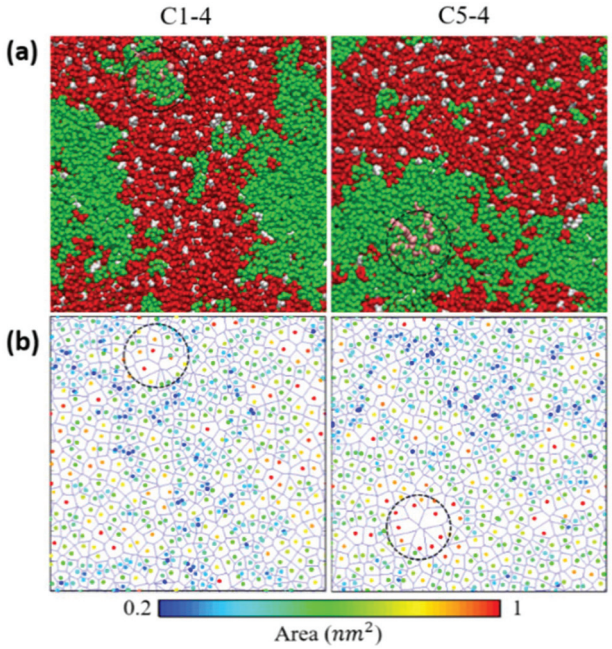

Fig. 5 The encapsulation of ligand-modified NPs affects the local area per lipid. (a) Top-view system snapshots at the end of 8 μs CGMD simulations (ligand hydrophobicity: C1/C5, ligand length: nl = 4, and ligand density: 100%). (b) Voronoi tessellation analysis of lipids in one monolayer at the end of 8 μs trajectories. The dots, which are colored with area per lipid, denote the COM of the DPPC/DUPC/CHOL groups. The coloring style of system snapshots is the same as in Fig. 1.

Local disturbance of embedded NPs on the phase-separated lipid membranes

As discussed before, the encapsulation of NPs into the lipid membrane does not have significant effects on the dynamics of the lipid raft. However, it may induce local disturbance to the membrane region around the NPs.[70] In order to capture these disturbances, we further used a 2D phase map which provides the detailed lipid distribution with chain order parameters (Fig. 4). From this time-evolution analysis, we could clearly found that saturated lipids became much more ordered during the phase-separation process of the lipid membrane, while the changes in the chain order of unsaturated lipids were not obvious. Moreover, in the case of ligand-modified NPs with high raft affinity, both in the upper and lower layer of the lipid membrane, chain order parameters of very surrounding lipids are smaller than those of the other saturated lipids in the raft domain, indicating that the encapsulation of the NP could induce local membrane curvature and make surrounding molecules disordered. However, this is not energy favorable for the saturated DPPC molecules compared to the unsaturated DUPC molecules, which have high chain flexibility. Hence, a few DUPC molecules were wrapped in the upper and lower regions of NPs to facilitate their membrane partitioning process as mentioned before.

In order to further capture structural disruptions induced by NPs, the Voronoi tessellation analysis was employed. The

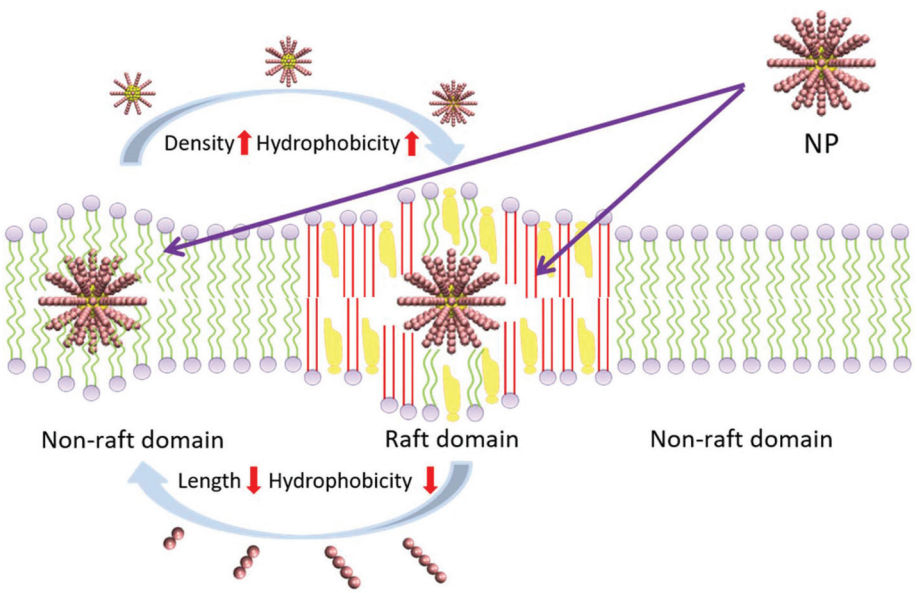

Scheme 1 Membrane localization preference of a hydrophobic ligand-modified NP is determined by its surface physicochemical properties.

COM coordinates of all the lipids in two membrane leaflets were used separately for the analysis. As shown in Fig. 5, for NPs with either high or low raft affinity, the area per lipid in the region where NPs were embedded was greatly increased. For NPs targeting the non-raft domain, the membrane even failed to fully encapsulate the ligand-modified NPs so that part of ligands directly exposed to the aqueous phase (right panel, Fig. 5). When NPs were located at the raft domain, the encapsulation degree was much better and the surrounding lipids consisted of DPPC, DUPC and Chol. On one hand, unsaturated lipids (DUPC) could facilitate DPPC and Chol to encapsulate NPs, which reduces the energy to induce local membrane curvature. On the other hand, the presence of DPPC and Chol made the local area per lipid around NPs much lower than that in the pure DUPC case (right panel, Fig. 5b).

Moreover, we also investigated the effects of ligand density and length of NPs on the thicknesses of raft and non-raft membrane domains. As shown in Fig. S7,† the encapsulation of the NP did not significantly change the overall thicknesses of either raft or non-raft membrane domains. However, ligand density and length jointly determined the local membrane thickness disturbance. In the case of the high ligand density and long ligand, the membrane thickness of the local area around the embedded NP is greatly increased. The effect of ligand density is much more obvious than that of ligand length. The differences in effects of these two factors on local membrane thickness disturbance are consistent with the local structural disruptions mentioned above, and can be ascribed to the NPs' size changes induced by these two factors.[66,67]

Conclusions

In this work, we studied the membrane partitioning dynamics of hydrophobic ligand-modified NPs by systematically changing the ligand hydrophobicity, length and density. We found that ligand hydrophobicity dominated NPs' raft affinity (Scheme 1). NPs of the higher hydrophobicity tend to partition into the raft domain, while NPs of the lower hydrophobicity prefer the non-raft domain. Ligand length and density are two important parameters that dominate the exposure degree of the NP core, which will affect the final partitioning dynamics of ligand-modified NPs. Besides, although these ultra-small NPs may induce certain local disturbances to the surrounding lipids, they generally have no obvious impact on the lipid raft dynamics, which may provide a new possibility for designing NP-based probes to target the raft domain. Considering the optical properties and stimuli-induced thermal effects of some inorganic NPs,[50,51] these NP-based probes may be used in imaging the raft domains and regulating their dynamics.

Conflicts of interest

There are no conflicts to declare.

Acknowledgements

This work was supported by the National Natural Science Foundation of China (No. 21903002 and 61821002), the Fundamental Research Funds for the Central Universities and the startup funds of Beijing Advanced Innovation Center for Biomedical Engineering. We thank the Supercomputing Center of Beihang University for generous computational resources.

References

1 S. Ray, A. Saha, N. R. Jana and R. Sarkar, Fluorescent Carbon Nanoparticles: Synthesis, Characterization, and Bioimaging Application, *J. Phys. Chem. C*, 2009, **113**, 18546–18551.
2 N. Erathodiyil and J. Y. Ying, Functionalization of Inorganic Nanoparticles for Bioimaging Applications, *Acc. Chem. Res.*, 2011, **44**, 925–935.
3 K. Riehemann, S. W. Schneider, T. A. Luger, B. Godin, M. Ferrari and H. Fuchs, Nanomedicine—Challenge and Perspectives, *Angew. Chem., Int. Ed.*, 2009, **48**, 872–897.
4 H. Chen, *et al.*, Precise Nanomedicine for Intelligent Therapy of Cancer, *Sci. China: Chem.*, 2018, **61**, 1503–1552.
5 G. Chen, I. Roy, C. Yang and P. N. Prasad, Nanochemistry and Nanomedicine for Nanoparticle-Based Diagnostics and Therapy, *Chem. Rev.*, 2016, **116**, 2826–2885.
6 W. Jiang, B. Y. Kim, J. T. Rutka and W. C. Chan, Nanoparticle-Mediated Cellular Response Is Size-Dependent, *Nat. Nanotechnol.*, 2008, **3**, 145–150.
7 A. Albanese, P. S. Tang and W. C. Chan, The Effect of Nanoparticle Size, Shape, and Surface Chemistry on Biological Systems, *Annu. Rev. Biomed. Eng.*, 2012, **14**, 1–16.
8 W. Wang, K. Gaus, R. D. Tilley and J. J. Gooding, The Impact of Nanoparticle Shape on Cellular Internalisation and Transport: What Do the Different Analysis Methods Tell Us?, *Mater. Horiz.*, 2019, **6**, 1538–1547.
9 K. Yang and Y.-Q. Ma, Computer Simulation of the Translocation of Nanoparticles with Different Shapes across a Lipid Bilayer, *Nat. Nanotechnol.*, 2010, **5**, 579–583.
10 X. Lin, Y. Y. Zuo and N. Gu, Shape Affects the Interactions of Nanoparticles with Pulmonary Surfactant, *Sci. China Mater.*, 2015, **58**, 28–37.
11 D. F. Moyano, M. Goldsmith, D. J. Solfiell, D. Landesman-Milo, O. R. Miranda, D. Peer and V. M. Rotello, Nanoparticle Hydrophobicity Dictates Immune Response, *J. Am. Chem. Soc.*, 2012, **134**, 3965–3967.
12 Y. Li, X. Chen and N. Gu, Computational Investigation of Interaction between Nanoparticles and Membranes: Hydrophobic/Hydrophilic Effect, *J. Phys. Chem. B*, 2008, **112**, 16647–16653.
13 X. Lin and N. Gu, Surface Properties of Encapsulating Hydrophobic Nanoparticles Regulate the Main Phase Transition Temperature of Lipid Bilayers: A Simulation Study, *Nano Res.*, 2014, **7**, 1195–1204.

14 Y. Zhang, N. Kohler and M. Zhang, Surface Modification of Superparamagnetic Magnetite Nanoparticles and Their Intracellular Uptake, *Biomaterials*, 2002, **23**, 1553–1561.

15 Z. Gu, S. H. Chen, Z. Ding, W. Song, W. Wei, S. Liu, G. Ma and R. Zhou, The Molecular Mechanism of Robust Macrophage Immune Responses Induced by Pegylated Molybdenum Disulfide, *Nanoscale*, 2019, **11**, 22293–22304.

16 A. E. Nel, L. Mädler, D. Velegol, T. Xia, E. M. Hoek, P. Somasundaran, F. Klaessig, V. Castranova and M. Thompson, Understanding Biophysicochemical Interactions at the Nano–Bio Interface, *Nat. Mater.*, 2009, **8**, 543–557.

17 Y. Wang, R. Cai and C. Chen, The Nano–Bio Interactions of Nanomedicines: Understanding the Biochemical Driving Forces and Redox Reactions, *Acc. Chem. Res.*, 2019, **52**, 1507–1518.

18 P. Zhao, N. Li and D. Astruc, State of the Art in Gold Nanoparticle Synthesis, *Coord. Chem. Rev.*, 2013, **257**, 638–665.

19 H. Duan, D. Wang and Y. Li, Green Chemistry for Nanoparticle Synthesis, *Chem. Soc. Rev.*, 2015, **44**, 5778–5792.

20 T. Casalini, V. Limongelli, M. Schmutz, C. Som, O. Jordan, P. Wick, G. Borchard and G. Perale, Molecular Modeling for Nanomaterial–Biology Interactions: Opportunities, Challenges, and Perspectives, *Front. Bioeng. Biotechnol.*, 2019, **7**, 268.

21 H. M. Ding and Y. Q. Ma, Theoretical and Computational Investigations of Nanoparticle–Biomembrane Interactions in Cellular Delivery, *Small*, 2015, **11**, 1055–1071.

22 X. Lu, P. Xu, H.-M. Ding, Y.-S. Yu, D. Huo and Y.-Q. Ma, Tailoring the Component of Protein Corona Via Simple Chemistry, *Nat. Commun.*, 2019, **10**, 1–14.

23 R. Cai and C. Chen, The Crown and the Scepter: Roles of the Protein Corona in Nanomedicine, *Adv. Mater.*, 2019, **31**, 1805740.

24 H.-M. Ding and Y.-Q. Ma, Computer Simulation of the Role of Protein Corona in Cellular Delivery of Nanoparticles, *Biomaterials*, 2014, **35**, 8703–8710.

25 A. J. Sodt, M. L. Sandar, K. Gawrisch, R. W. Pastor and E. Lyman, The Molecular Structure of the Liquid-Ordered Phase of Lipid Bilayers, *J. Am. Chem. Soc.*, 2014, **136**, 725–732.

26 R. M. Venable, A. Krämer and R. W. Pastor, Molecular Dynamics Simulations of Membrane Permeability, *Chem. Rev.*, 2019, **119**, 5954–5997.

27 H.-M. Ding and Y.-Q. Ma, Role of Physicochemical Properties of Coating Ligands in Receptor-Mediated Endocytosis of Nanoparticles, *Biomaterials*, 2012, **33**, 5798–5802.

28 G. Van Meer, D. R. Voelker and G. W. Feigenson, Membrane Lipids: Where They Are and How They Behave, *Nat. Rev. Mol. Cell Biol.*, 2008, **9**, 112–124.

29 L. Wang, *et al.*, Stability of Ligands on Nanoparticles Regulating the Integrity of Biological Membranes at the Nano–Lipid Interface, *ACS Nano*, 2019, **13**, 8680–8693.

30 F. A. Heberle, R. S. Petruzielo, J. Pan, P. Drazba, N. Kučerka, R. F. Standaert, G. W. Feigenson and J. Katsaras, Bilayer Thickness Mismatch Controls Domain Size in Model Membranes, *J. Am. Chem. Soc.*, 2013, **135**, 6853–6859.

31 X. Cheng and J. C. Smith, Biological Membrane Organization and Cellular Signaling, *Chem. Rev.*, 2019, **119**, 5849–5880.

32 G. Enkavi, M. Javanainen, W. Kulig, T. Róg and I. Vattulainen, Multiscale Simulations of Biological Membranes: The Challenge to Understand Biological Phenomena in a Living Substance, *Chem. Rev.*, 2019, **119**, 5607–5774.

33 E. Sezgin, I. Levental, S. Mayor and C. Eggeling, The Mystery of Membrane Organization: Composition, Regulation and Roles of Lipid Rafts, *Nat. Rev. Mol. Cell Biol.*, 2017, **18**, 361–374.

34 M. n. M. Lozano, J. S. Hovis, F. R. Moss III and S. G. Boxer, Dynamic Reorganization and Correlation among Lipid Raft Components, *J. Am. Chem. Soc.*, 2016, **138**, 9996–10001.

35 B. B. Diaz-Rohrer, K. R. Levental, K. Simons and I. Levental, Membrane Raft Association Is a Determinant of Plasma Membrane Localization, *Proc. Natl. Acad. Sci. U. S. A.*, 2014, **111**, 8500–8505.

36 X. Lin and A. A. Gorfe, Understanding Membrane Domain-Partitioning Thermodynamics of Transmembrane Domains with Potential of Mean Force Calculations, *J. Phys. Chem. B*, 2019, **123**, 1009–1016.

37 L. Janosi, Z. Li, J. F. Hancock and A. A. Gorfe, Organization, Dynamics, and Segregation of Ras Nanoclusters in Membrane Domains, *Proc. Natl. Acad. Sci. U. S. A.*, 2012, **109**, 8097–8102.

38 Z. Li, L. Janosi and A. A. Gorfe, Formation and Domain Partitioning of H-Ras Peptide Nanoclusters: Effects of Peptide Concentration and Lipid Composition, *J. Am. Chem. Soc.*, 2012, **134**, 17278–17285.

39 X. Lin, J. H. Lorent, A. D. Skinkle, K. R. Levental, M. N. Waxham, A. A. Gorfe and I. Levental, Domain Stability in Biomimetic Membranes Driven by Lipid Polyunsaturation, *J. Phys. Chem. B*, 2016, **120**, 11930–11941.

40 H.-J. Kaiser, D. Lingwood, I. Levental, J. L. Sampaio, L. Kalvodova, L. Rajendran and K. Simons, Order of Lipid Phases in Model and Plasma Membranes, *Proc. Natl. Acad. Sci. U. S. A.*, 2009, **106**, 16645–16650.

41 J. D. Nickels, J. C. Smith and X. Cheng, Lateral Organization, Bilayer Asymmetry, and, Inter-Leaflet Coupling of Biological Membranes, *Chem. Phys. Lipids*, 2015, **192**, 87–99.

42 X. Lin, S. Zhang, H. Ding, I. Levental and A. A. Gorfe, The Aliphatic Chain of Cholesterol Modulates Bilayer Interleaflet Coupling and Domain Registration, *FEBS Lett.*, 2016, **590**, 3368–3374.

43 S. Zhang and X. Lin, Lipid Acyl Chain Cis Double Bond Position Modulates Membrane Domain Registration/Anti-Registration, *J. Am. Chem. Soc.*, 2019, **141**, 15884–15890.

44 W.-D. Tian and Y.-Q. Ma, Theoretical and Computational Studies of Dendrimers as Delivery Vectors, *Chem. Soc. Rev.*, 2013, **42**, 705–727.

45 P. Chen, H. Yue, X. Zhai, Z. Huang, G.-H. Ma, W. Wei and L.-T. Yan, Transport of a Graphene Nanosheet Sandwiched inside Cell Membranes, *Sci. Adv.*, 2019, **5**, eaaw3192.

46 Y. Tu, M. Lv, P. Xiu, T. Huynh, M. Zhang, M. Castelli, Z. Liu, Q. Huang, C. Fan and H. Fang, Destructive Extraction of Phospholipids from Escherichia Coli Membranes by Graphene Nanosheets, *Nat. Nanotechnol.*, 2013, **8**, 594–601.

47 T. Yue and X. Zhang, Molecular Understanding of Receptor-Mediated Membrane Responses to Ligand-Coated Nanoparticles, *Soft Matter*, 2011, **7**, 9104–9112.

48 X. Chen, D. P. Tieleman and Q. Liang, Modulating Interactions between Ligand-Coated Nanoparticles and Phase-Separated Lipid Bilayers by Varying the Ligand Density and the Surface Charge, *Nanoscale*, 2018, **10**, 2481–2491.

49 J. Wong-Ekkabut, S. Baoukina, W. Triampo, I.-M. Tang, D. P. Tieleman and L. Monticelli, Computer Simulation Study of Fullerene Translocation through Lipid Membranes, *Nat. Nanotechnol.*, 2008, **3**, 363–368.

50 A. J. Mieszawska, W. J. M. Mulder, Z. A. Fayad and D. P. Cormode, Multifunctional Gold Nanoparticles for Diagnosis and Therapy of Disease, *Mol. Pharmaceutics*, 2013, **10**, 831–847.

51 N. Lee, D. Yoo, D. Ling, M. H. Cho, T. Hyeon and J. Cheon, Iron Oxide Based Nanoparticles for Multimodal Imaging and Magnetoresponsive Therapy, *Chem. Rev.*, 2015, **115**, 10637–10689.

52 S. J. Marrink, A. H. De Vries and A.,E. Mark, Coarse Grained Model for Semiquantitative Lipid Simulations, *J. Phys. Chem. B*, 2004, **108**, 750–760.

53 S. J. Marrink, H. J. Risselada, S. Yefimov, D. P. Tieleman and A. H. De Vries, The Martini Force Field: Coarse Grained Model for Biomolecular Simulations, *J. Phys. Chem. B*, 2007, **111**, 7812–7824.

54 H. J. Risselada and S. J. Marrink, The Molecular Face of Lipid Rafts in Model Membranes, *Proc. Natl. Acad. Sci. U. S. A.*, 2008, **105**, 17367–17372.

55 L. V. Schäfer, D. H. de Jong, A. Holt, A. J. Rzepiela, A. H. de Vries, B. Poolman, J. A. Killian and S. J. Marrink, Lipid Packing Drives the Segregation of Transmembrane Helices into Disordered Lipid Domains in Model Membranes, *Proc. Natl. Acad. Sci. U. S. A.*, 2011, **108**, 1343–1348.

56 A. J. Pak and G. A. Voth, Advances in Coarse-Grained Modeling of Macromolecular Complexes, *Curr. Opin. Struct. Biol.*, 2018, **52**, 119–126.

57 L. Zhang and X. Wang, Coarse-Grained Modeling of Vesicle Responses to Active Rotational Nanoparticles, *Nanoscale*, 2015, **7**, 13458–13467.

58 L. Zhang, Y. Zhao and X. Wang, Nanoparticle-Mediated Mechanical Destruction of Cell Membranes: A Coarse-Grained Molecular Dynamics Study, *ACS Appl. Mater. Interfaces*, 2017, **9**, 26665–26673.

59 S. Pronk, S. Páll, R. Schulz, P. Larsson, P. Bjelkmar, R. Apostolov, M. R. Shirts, J. C. Smith, P. M. Kasson and D. Van Der Spoel, GROMACS 4.5: A High-Throughput and Highly Parallel Open Source Molecular Simulation Toolkit, *Bioinformatics*, 2013, **29**, 845–854.

60 G. Bussi, D. Donadio and M. Parrinello, Canonical Sampling through Velocity Rescaling, *J. Chem. Phys.*, 2007, **126**, 014101.

61 M. Parrinello and A. Rahman, Polymorphic Transitions in Single Crystals: A New Molecular Dynamics Method, *J. Appl. Phys.*, 1981, **52**, 7182–7190.

62 W. Humphrey, A. Dalke and K. Schulten, VMD: Visual Molecular Dynamics, *J. Mol. Graphics*, 1996, **14**, 33–38.

63 S. J. Marrink and D. P. Tieleman, Perspective on the Martini Model, *Chem. Soc. Rev.*, 2013, **42**, 6801–6822.

64 T. A. Wassenaar, H. I. Ingólfsson, R. A. Böckmann, D. P. Tieleman and S. J. Marrink, Computational Lipidomics with Insane: A Versatile Tool for Generating Custom Membranes for Molecular Simulations, *J. Chem. Theory Comput.*, 2015, **11**, 2144–2155.

65 J. H. Lorent, B. Diaz-Rohrer, X. Lin, K. Spring, A. A. Gorfe, K. R. Levental and I. Levental, Structural Determinants and Functional Consequences of Protein Affinity for Membrane Rafts, *Nat. Commun.*, 2017, **8**, 1219.

66 H. Liu, H.-Y. Zhao, F. Müller-Plathe, H.-J. Qian, Z.-Y. Sun and Z.-Y. Lu, Distribution of the Number of Polymer Chains Grafted on Nanoparticles Fabricated by Grafting-to and Grafting-from Procedures, *Macromolecules*, 2018, **51**, 3758–3766.

67 R. Shi, H.-J. Qian and Z.-Y. Lu, Tuning Cavitation and Crazing in Polymer Nanocomposite Glasses Containing Bimodal Grafted Nanoparticles at the Nanoparticle/Polymer Interface, *Phys. Chem. Chem. Phys.*, 2019, **21**, 7115–7126.

68 V. V. Ginzburg, Modeling the Morphology and Phase Behavior of One-Component Polymer-Grafted Nanoparticle Systems, *Macromolecules*, 2017, **50**, 9445–9455.

69 A. Huerre, F. Cacho-Nerin, V. Poulichet, C. E. Udoh, M. De Corato and V. Garbin, Dynamic Organization of Ligand-Grafted Nanoparticles During Adsorption and Surface Compression at Fluid–Fluid Interfaces, *Langmuir*, 2018, **34**, 1020–1028.

70 R. Qiao, A. P. Roberts, A. S. Mount, S. J. Klaine and P. C. Ke, Translocation of C60 and Its Derivatives across a Lipid Bilayer, *Nano Lett.*, 2007, **7**, 614–619.